

https://dspace.org/

Insights into the VakhnenkoParkes equation solitary waves under the influence of powerlaw nonlinearity

A Turgut; S Dhawan; M Khater; Abdul Kara

INDIAN ACAD SCIENCES
https://hdl.handle.net/10539/46965
WOS

Downloaded from a DSpace repository. https://dspace.org/

Pramana – J. Phys. (2025) 99:71
https://doi.org/10.1007/s12043-025-02929-0
© Indian Academy of Sciences

Insights into the Vakhnenko–Parkes equation: solitary waves under the influence of power-law nonlinearity

TURGUT AK[1,*], SHARANJEET DHAWAN[2], MOSTAFA M A KHATER[3,4,5] and ABDUL HAMID KARA[6]

[1]Department of Basic Sciences, Turkish Air Force Academy, National Defence University, 34149 Istanbul, Türkiye
[2]Department of Mathematics, College of Agriculture, Chaudhary Charan Singh Haryana Agricultural University, 123501 Haryana, India
[3]School of Medical Informatics and Engineering, Xuzhou Medical University, 221004 Xuzhou, Jiangsu Province, People's Republic of China
[4]Institute of Digital Economy, Ugra State University, 628012 Khanty-Mansiysk, Russia
[5]Department of Basic Science, The Higher Institute for Engineering & Technology, Cairo 10587, Egypt
[6]School of Mathematics, University of the Witwatersrand, Johannesburg 2050, South Africa
*Corresponding author. E-mail: akturgut@yahoo.com

MS received 14 August 2024; revised 10 December 2024; accepted 19 February 2025

Abstract. In this study, we identify two distinct families of solutions for the Vakhnenko–Parkes (VP) equation using a hybrid computational scheme. This methodology, referred to as the hybrid scheme, integrates B-spline functions with a finite-element approach. The notable advantage of this scheme is its unconditional stability, which enables the successful development of both topological and non-topological solutions. To demonstrate its efficacy, several test cases are examined. We visualise the dynamics of topological and non-topological solitary wave profiles by presenting results through figures and calculating the associated errors. Furthermore, we derive an analytical solution using the Khater II technique and compute conservation laws. In summary, our findings suggest that the presented scheme is highly effective and adaptable to various other nonlinear models.

Keywords. B-spline; collocation; solitary wave; Vakhnenko–Parkes equation.

PACS Nos. **02.60.Cb; 02.70.–c; 11.30.–j; 44.05.+e; 47.11.–j; 47.35.Fg**

1. Introduction

Nonlinear evolution equations constitute an integral component of numerous real-world problems. This is attributable to the fact that the modelling of various real-world phenomena frequently results in nonlinear partial differential equation models. Consequently, physicists, mathematicians and biologists are actively engaged in developing diverse techniques to solve these models. In the study of solitons, the Vakhnenko–Parkes (VP) equation is a prominent nonlinear partial differential equation. Its solitary wave solutions exhibit periodic characteristics, rendering it capable of describing a multitude of physical phenomena. Key areas of interest encompass fluid dynamics, optical fibres, plasma physics and related fields. A critical aspect of investigating these solutions involves exploring both topological and non-topological solutions.

The literature survey elucidates various solution techniques devised to address the VP equation [1–6]. Notably, Liu and He employed the improved (G'/G) expansion method [7]. They transformed the independent variable and subsequently utilised Hirota's method [8], leading to the discovery of the N-soliton solution.

Novel coherent structures, including soliton-type, instanton-type and rogue wave-type solutions, have been established [9]. Additionally, Majid et al employed the ansatz method to solve the VP equation, providing an alternative approach [10]. Ma et al investigated another set of solutions for the modified Vakhnenko equation [11]. Furthermore, Wazwaz made significant contributions to the development of multiple real and complex solutions [12].

Building upon the literature survey of the VP equation, our current focus is to investigate both non-topological and topological solutions using a combined

Published online: 26 May 2025

approach. This method integrates cubic B-splines with the finite-element method (FEM).

The paper is organised as follows: Section 2 introduces the mathematical model under observation, followed by §3 presenting the analytical solutions. Section 4 details the calculations of conserved quantities via conservation laws. Section 5 concentrates on numerical simulations, outlining the implementation of the proposed scheme on various test cases. This segment elaborates on the procedure, discussing the fundamental construction of cubic B-splines and our use of the finite-element approach. It encompasses stability analysis and the graphical representation of results. In §6, physical systems and experimental set-ups in which the obtained solutions can be observed are discussed. Finally, §7 draws conclusions, followed by a list of references that motivated our work.

2. Mathematical modelling

A general expression for the VP equation is

$$u\frac{\partial}{\partial t}\left(\frac{\partial^2 u}{\partial x^2}\right)-\frac{\partial u}{\partial x}\frac{\partial}{\partial t}\left(\frac{\partial u}{\partial x}\right)+u^2\frac{\partial u}{\partial t}=0. \tag{1}$$

But, in the present work, we are concerned about the VP model with the power-law nonlinearity

$$u\frac{\partial}{\partial t}\left(\frac{\partial^2 u}{\partial x^2}\right)+a\frac{\partial u}{\partial x}\frac{\partial}{\partial t}\left(\frac{\partial u}{\partial x}\right)+bu^{2p}\frac{\partial u}{\partial t}=0,\quad p\in Z^+. \tag{2}$$

Additionally, a and b represent non-zero real constants [10]. The parameter p denotes the power-law nonlinearity. By focussing on specific values of a, b and p, we observe that eq. (2) reduces to eq. (1) when $a=-1$, $b=1$ and $p=1$. Major aspects of this work involve the development of two families of solutions. Moreover, the power-law nonlinearity parameter p is of particular interest because the dynamics of this problem are significantly influenced by p. The implementation of the proposed technique confirms the development of non-topological solitary waves for any exponent $p>\frac{1}{2}$ and topological solitary waves for $p=\frac{3}{2}$.

These targets are achieved with the help of numerical scheme presented in the following sections.

3. Analytical solutions

Implementing Khater II technique to eq. (2) along with the transformation $u(x,t)=\varphi(\eta)$, $\eta=\sigma t+x$, where σ is arbitrary constant, converts the nonlinear PDE into the next nonlinear ODE of the form

$$(2p+1)\left((a-1)\varphi'^2+2\varphi\varphi''\right)+2b\varphi^{2p+1}=0. \tag{3}$$

Balancing the highest-order derivative term and nonlinear term by using the next rule

$$\begin{aligned} D\left[\frac{\mathrm{d}^q\varphi}{\mathrm{d}\eta^q}\right]&=n+q,\\ D\left[\varphi^p\left(\frac{\mathrm{d}^q\varphi}{\mathrm{d}\eta^q}\right)^s\right]&=np+s(n+q), \end{aligned} \tag{4}$$

we get

$$n=\frac{2}{2p-1}.$$

Thus, we have to use another transformation

$$\varphi=\phi^{\frac{2}{2p-1}},$$

that converts eq. (3) into the following ODE:

$$\begin{aligned} &4(2p+1)\left((a-2p+2)\left(\phi'\right)^2+(2p-1)\phi\phi''\right)\\ &\quad+2b(1-2p)^2\phi^4=0. \end{aligned} \tag{5}$$

Again, determining the balance value between ϕ^4 and $\phi\phi''$, the general solution of eq. (5) is given by

$$\phi(\eta)=\sum_{i=1}^{n}\left(a_i f(\eta)^i+b_i\phi(\eta)f(\eta)^{i-1}\right)+a_0, \tag{6}$$

where a_0, a_1 and b_1 are unknown quantities yet to be determined. Putting eq. (6) along with its derivatives into eq. (5) and after some computations, we have the following system of equations that is solved using Mathematica 13.1 as

$$a_0\to 0,\quad a_1\to 0,\quad a\to -1,\quad b\to -\frac{2(\delta+2\delta p)}{b_1^2(2p-1)}.$$

Thus, with power-law nonlinearity, we get the solutions of the VP equation as

$$u(x,t)=\left(b_1\sec\left[\sqrt{\delta}(x+\sigma t)\right]\right)^{\frac{2}{2p-1}}, \tag{7}$$

$$u(x,t)=\left(b_1\csc\left[\sqrt{\delta}(x+\sigma t)\right]\right)^{\frac{2}{2p-1}}. \tag{8}$$

Non-topological solitary wave solutions and travelling wave solutions are depicted in detail in figures 1 and 2, respectively.

4. Conservation laws

Here, we calculate conservation laws for eq. (2). The conserved flow (T^t, T^x) satisfying the conserved form

$$D_t T^t+D_x T^x=0|_{uu_{xxt}+au_xu_{xt}+bu^6u_t=0} \tag{9}$$

can be obtained with the help of 'multiplier technique' in which

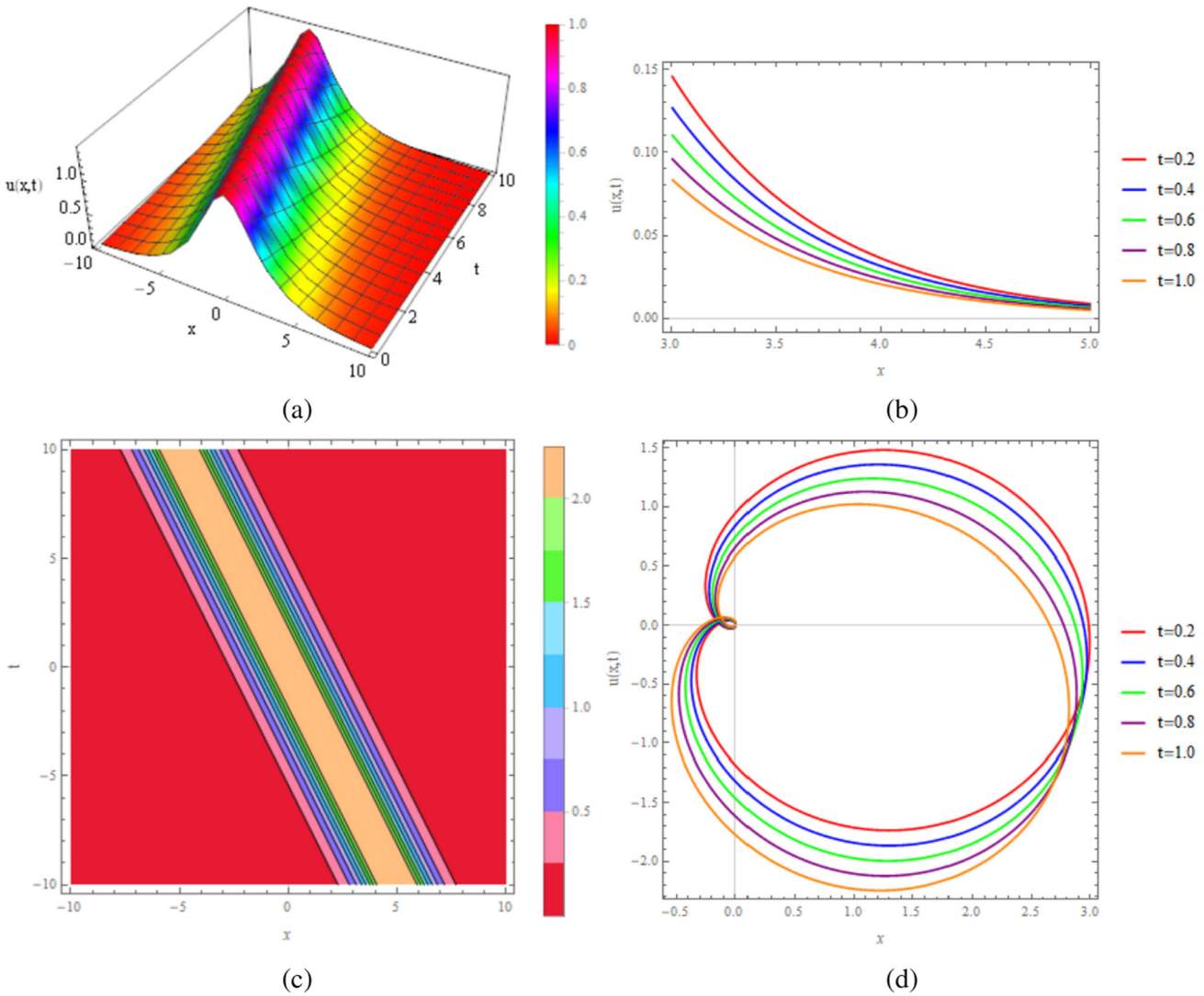

Figure 1. Non-topological solitary wave representations of eq. (7) for $a = -1$, $b = 1$, $p = 1$, $\sigma = 0.5$ and $\delta = -0.5$. (**a**) 3D plot, (**b**) 2D plot, (**c**) contour plot and (**d**) polar plot.

$$D_t T^t + D_x T^x = Q\,(x, t, u, \ldots) \times \left(uu_{xxt} + au_x u_{xt} + bu^6 u_t\right), \quad (10)$$

for some differential function $Q\,(x, t, u, u_x, u_t, \ldots)$ where Q can be obtained from

$$\mathcal{E}\left[Q\,(x, t, u, \ldots)\left(uu_{xxt} + au_x u_{xt} + bu^{2p} u_t\right)\right] = 0, \quad (11)$$

where $\mathcal{E}$ is the Euler operator [13,14] (figure 1 and 2). Then, we get the components of the conserved flow with the following multipliers:

(i) $Q_1 = 1$:

$$T_1^t = -\frac{1}{1+2p} bu^{1+2p} - \frac{1}{4}au_x^2 + \frac{1}{4}auu_{xx} - \frac{1}{3}uu_{xx},$$
$$T_1^x = -\left(\frac{1}{4}au_x u_t + \frac{1}{4}auu_{xt} + \frac{2}{3}uu_{xt}\right). \quad (12)$$

(ii) $Q_2 = u^{a-1}$:

$$T_2^t = -\frac{1}{1+2p} bu^{a-1}u^{1+2p} - \frac{1}{4}au^{a-1}u_x^2 + \frac{1}{4}auu^{a-1}u_{xx} - \frac{1}{3}u^a u_{xx}, \quad (13)$$
$$T_2^x = -\left(\frac{1}{4}au^{a-1}u_x u_t + \frac{1}{4}auu^{a-1}u_{xt} + \frac{2}{3}u^a u_{xt}\right).$$

The conserved quantities are calculated using

$$C_1 = \int_{-\infty}^{\infty} T_1^t \mathrm{d}x = \int_{-\infty}^{\infty} \left[-\frac{1}{1+2p} bu^{1+2p} - \frac{1}{4}au_x^2 + \frac{1}{4}auu_{xx} - \frac{1}{3}uu_{xx}\right] \mathrm{d}x,$$

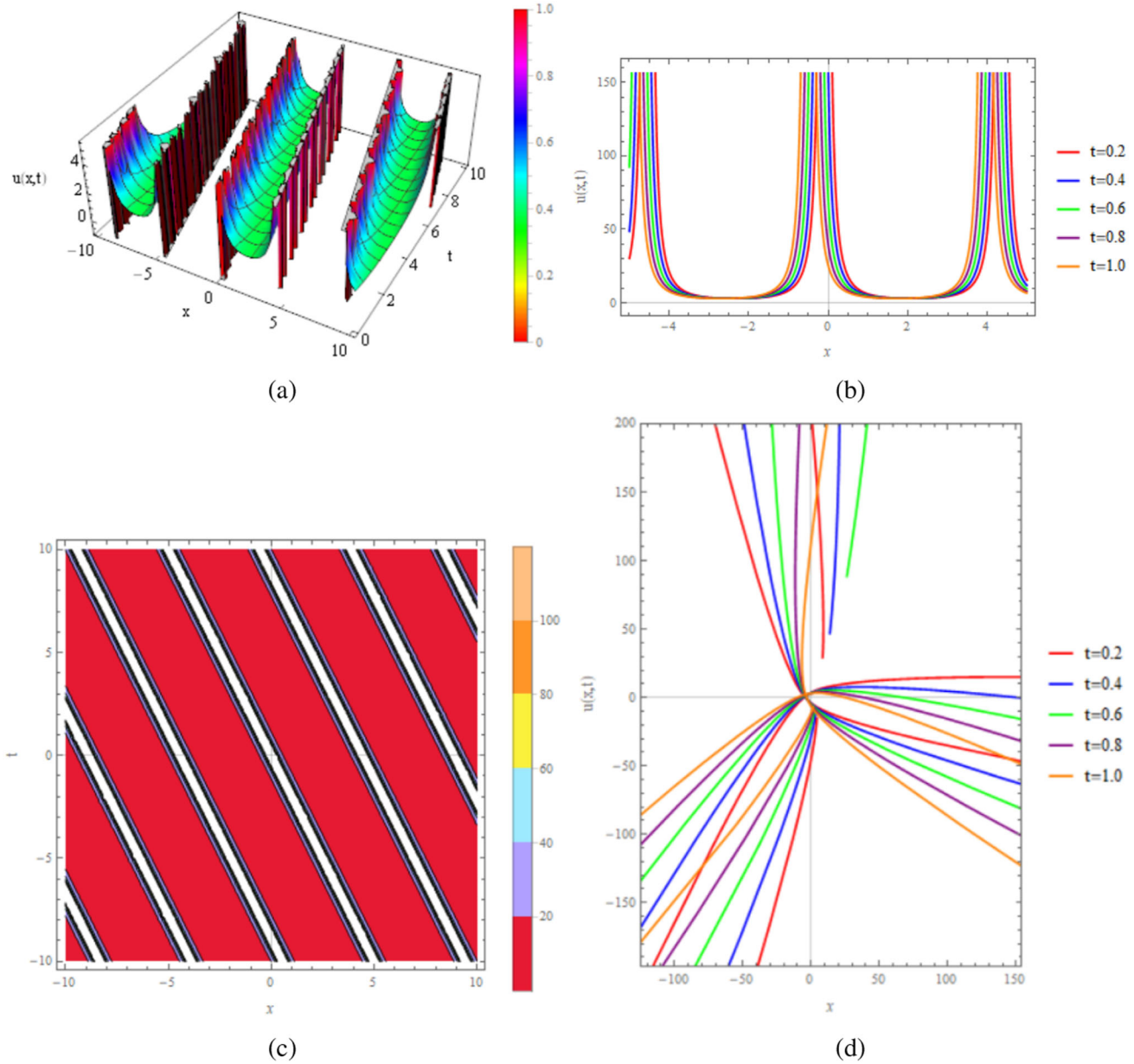

Figure 2. Travelling wave representations of eq. (8) for $a = -1$, $b = -1$, $p = 1$, $\sigma = 0.5$ and $\delta = 0.5$. (**a**) 3D plot, (**b**) 2D plot, (**c**) contour plot and (**d**) polar plot.

$$C_2 = \int_{-\infty}^{\infty} T_2^t \mathrm{d}x = \int_{-\infty}^{\infty} \left[-\frac{1}{1+2p} b u^{a-1} u^{1+2p} - \frac{1}{4} a u^{a-1} u_x^2 + \frac{1}{4} a u u^{a-1} u_{xx} - \frac{1}{3} u^a u_{xx} \right] \mathrm{d}x, \tag{14}$$

respectively.

5. Numerical simulations

This section is dedicated to the proposed computational approach, which integrates B-spline functions with the FEM. Compared to other numerical approaches employed by various researchers, B-spline functions garner more attention due to their attractive properties. Additional details about B-spline functions can be found in refs [15–17]. However, the basic definition of the cubic B-splines implemented in this work is as follows.

5.1 *Preliminaries*

The cubic B-spline functions (CBSF) over the interval $[x_L, x_R]$ for $m = -1(1)N + 1$ are defined as follows:

$$\phi_m(x) = \frac{1}{h^3}\begin{cases} (x - x_{m-2})^3, & x \in [x_{m-2}, x_{m-1}], \\ h^3 + 3h^2(x - x_{m-1}) + 3h(x - x_{m-1})^2 - 3(x - x_{m-1})^3, & x \in [x_{m-1}, x_m], \\ h^3 + 3h^2(x_{m+1} - x) + 3h(x_{m+1} - x)^2 - 3(x_{m+1} - x)^3, & x \in [x_m, x_{m+1}], \\ (x_{m+2} - x)^3, & x \in [x_{m+1}, x_{m+2}], \\ 0, & \text{elsewhere}, \end{cases} \tag{15}$$

where x_m's are the knots [18]. The functions $\phi_m(x)$ over the interval $[x_{m-2}, x_{m+2}]$ are presented in table 1. We can observe from the table that $\phi_m(x)$ and its two basic derivatives are zero except at $[x_{m-2}, x_{m+2}]$.

In addition, the CBSFs over a typical interval $[x_m, x_{m+1}]$ are shown in figure 3. It shows that every element is involving four CBSFs. Likewise, each CBSF covers four elements [18].

Lemma 1. *The functions* $\{\phi_{-1}(x), \phi_0(x), \ldots, \phi_{N+1}(x)\}$ *formulate a basis. Based on this,* $u_N(x, t)$ *solution approaching the analytical results generated by* $\phi_j(x)$ element shape functions and $\delta_j(t)$.

Table 1. CBSF and its two basic derivatives at nodes x_m.

x	x_{m-2}	x_{m-1}	x_m	x_{m+1}	x_{m+2}
$\phi_m(x)$	0	1	4	1	0
$h\phi'_m(x)$	0	−3	0	3	0
$h^2\phi''_m(x)$	0	6	−12	6	0

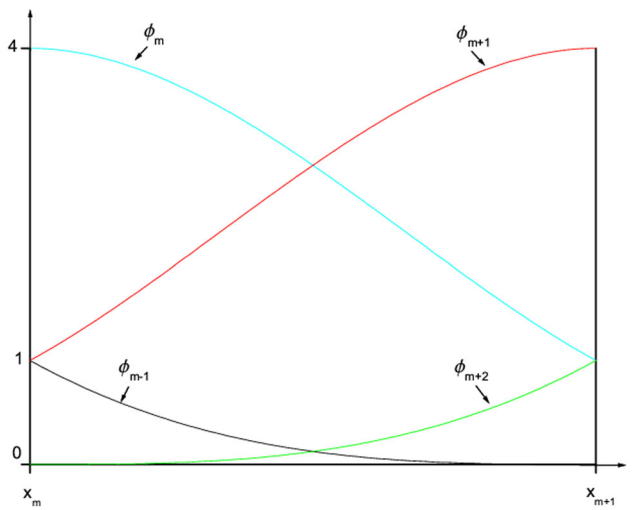

Figure 3. A graphical representation of the CBSFs.

$$u_N(x, t) = \sum_{j=-1}^{N+1} \phi_j(x)\delta_j(t), \tag{16}$$

Lemma 2. $u(x, t)$ *function and its derivatives at knot* x_m *are stated as*

$$\begin{aligned} u_m &= u(x_m) = \delta_{m-1} + 4\delta_m + \delta_{m+1}, \\ u'_m &= u'(x_m) = \frac{3}{h}(-\delta_{m-1} + \delta_{m+1}), \\ u''_m &= u''(x_m) = \frac{6}{h^2}(\delta_{m-1} - 2\delta_m + \delta_{m+1}). \end{aligned} \tag{17}$$

5.2 *Implementation of the finite-element method*

Nowadays, FEM is playing a vital role in solving plenty of models. Keeping in view the efficiency of FEMs to solve mathematical models, we have used this approach in the present work. A few introductory sentences are given here.

For the solution process, we line off the solution domain to an interval $x_L \le x \le x_R$. Then, this interval $[x_L, x_R]$ is discretised into elements of equal size

$$h = \frac{x_R - x_L}{N}$$

with help of the knots x_m for $m = 0, 1, 2, \ldots, N$ such as $x_L = x_0 < x_1 < \cdots < x_N = x_R$.

If eq. (17) is used in eq. (2), the following equality is obtained:

$$\begin{aligned} &(\delta_{m-1} + 4\delta_m + \delta_{m+1})\left[\frac{6}{h^2}\left(\dot{\delta}_{m-1} - 2\dot{\delta}_m + \dot{\delta}_{m+1}\right)\right] \\ &\quad + a\left[\frac{3}{h}(-\delta_{m-1} + \delta_{m+1})\right]\left[\frac{3}{h}\left(-\dot{\delta}_{m-1} + \dot{\delta}_{m+1}\right)\right] \\ &\quad + b\,(\delta_{m-1} + 4\delta_m + \delta_{m+1})^{2p}\left(\dot{\delta}_{m-1} + 4\dot{\delta}_m + \dot{\delta}_{m+1}\right) \\ &\quad = 0. \end{aligned} \tag{18}$$

When eq. (18) is arranged, we have

$$\begin{aligned} &z_1\left[\frac{6}{h^2}\left(\dot{\delta}_{m-1} - 2\dot{\delta}_m + \dot{\delta}_{m+1}\right)\right] \\ &+ az_2\frac{9}{h^2}\left(-\dot{\delta}_{m-1} + \dot{\delta}_{m+1}\right) \\ &+ bz_3\left(\dot{\delta}_{m-1} + 4\dot{\delta}_m + \dot{\delta}_{m+1}\right) = 0, \end{aligned} \tag{19}$$

where

$$\begin{aligned} z_1 &= u_m = (\delta_{m-1} + 4\delta_m + \delta_{m+1}), \\ z_2 &= \frac{h}{3}u'_m = (-\delta_{m-1} + \delta_{m+1}), \\ z_3 &= u_m^{2p} = (\delta_{m-1} + 4\delta_m + \delta_{m+1})^{2p}, \end{aligned} \tag{20}$$

and $\cdot$ denotes the differentiation with respect to t. To linearise eq. (2), the term u in the non-linear terms uu_{xxt}, the term $\frac{h}{3}u_x$ and the term u^{2p} are assumed to behave like a constant quantity.

With the help of Crank–Nicolson finite-difference approximation and the forward difference approach, we have

$$\delta_i = \frac{\delta_i^{n+1} + \delta_i^n}{2}, \quad \dot{\delta}_i = \frac{\delta_i^{n+1} - \delta_i^n}{\Delta t}. \tag{21}$$

Using this approximation, we obtain the recurrence relation

$$\gamma_1\delta_{m-1}^{n+1} + \gamma_2\delta_m^{n+1} + \gamma_3\delta_{m+1}^{n+1} = \gamma_1\delta_{m-1}^n + \gamma_2\delta_m^n + \gamma_3\delta_{m+1}^n, \tag{22}$$

for $i = m-2, m-1, \ldots, m+1, m+2$. Here, the coefficients are figured out as

$$\begin{aligned} \gamma_1 &= [Az_1 - Bz_2 + Cz_3], \\ \gamma_2 &= [-2Az_1 + 4Cz_3], \\ \gamma_3 &= [Az_1 + Bz_2 + Cz_3], \end{aligned} \tag{23}$$

where

$$A = \frac{6}{h^2}, \quad B = \frac{9}{h^2}a, \quad C = b$$

for $m = 0, 1, \ldots, N$.

To get the solution of the system in hand, we need to eliminate unknown quantities δ_{-1} and δ_{N+1} by making use of boundary conditions in system (22) consisting of linear equations with $(N+3)$ quantities yet to be determined. In that case, system (22) turns into shade the matrix form as

$$H\mathbf{d^{n+1}} = K\mathbf{d^n}, \tag{24}$$

where $d = (\delta_0, \delta_1, \ldots, \delta_N)^T$, H and K are $(N+1) \times (N+1)$ tridiagonal matrices. Afterwards, matrix equation (24) is solved by taking advantage of the tridiagonal procedure. To overcome the nonlinearity effect caused by nonlinear terms in eq. (2), inner iteration is performed twice with the term $\delta^{n*} = \delta^n + \frac{1}{2}(\delta^n - \delta^{n-1})$ at each step of the time. To start with the initial step, we have the matrix form as

$$W\mathbf{d^0} = L, \tag{25}$$

where $\mathbf{d^0} = (\delta_0, \delta_1, \ldots, \delta_{N-1}, \delta_N)$ is the initial vector and we use initial and following boundary conditions

$$\begin{aligned} &(u_N)_x(x_L, 0) = 0, \quad (u_N)_x(x_R, 0) = 0, \\ &(u_N)_{xx}(x_L, 0) = 0, \quad (u_N)_{xx}(x_R, 0) = 0. \end{aligned} \tag{26}$$

This matrix system (25) can be clearly written as follows:

$$\begin{bmatrix} 4 & 2 & & & & \\ 1 & 4 & 1 & & & \\ & 1 & 4 & 1 & & \\ & & \ddots & & & \\ & & & 1 & 4 & 1 \\ & & & & 1 & 4 & 1 \\ & & & & & 2 & 4 \end{bmatrix} \begin{bmatrix} \delta_0 \\ \delta_1 \\ \delta_2 \\ \vdots \\ \delta_{N-2} \\ \delta_{N-1} \\ \delta_N \end{bmatrix} = \begin{bmatrix} U(x_0, 0) \\ U(x_1, 0) \\ U(x_2, 0) \\ \vdots \\ U(x_{N-2}, 0) \\ U(x_{N-1}, 0) \\ U(x_N, 0) \end{bmatrix}.$$

Lastly, we solve this matrix system in hand.

5.3 *Stability of the numerical scheme*

We performed the stability analysis for the linearised computational technique for gVP equation (2) with the help of the von Neumann theory using the Fourier mode

$$\delta_m^n = \xi^n e^{imkh}, \tag{27}$$

where ξ represents the growth factor for the error in a special mode of amplitude ξ^n, h represents the step size and k denotes mode number. If Fourier mode (27) is inserted into system (22), the following equality

$$\begin{aligned} &\gamma_1\xi^{n+1}e^{i(m-1)kh} + \gamma_2\xi^{n+1}e^{imkh} + \gamma_3\xi^{n+1}e^{i(m+1)kh} \\ &= \gamma_1\xi^n e^{i(m-1)kh} + \gamma_2\xi^n e^{imkh} + \gamma_3\xi^n e^{i(m+1)kh} \end{aligned} \tag{28}$$

is obtained. If the Euler's formula is replaced into eq. (28), upon simplification, the growth factor is computed as

$$\xi = \frac{\omega - i\varpi}{\omega + i\varpi}, \tag{29}$$

where

$$\begin{aligned} \omega &= 2[Az_1 + Cz_3]\cos(kh) - 2[Az_1 - 2Cz_3], \\ \varpi &= -2Bz_2\sin(kh). \end{aligned} \tag{30}$$

Since $|\xi| = 1$, we observe that our method is unconditionally stable.

5.4 *Numerical results*

To investigate the efficient working of the proposed computational scheme, we consider two examples in this section. We compute error norms

$$L_2 = \left\|u^{\text{exact}} - u_N\right\|_2 \simeq \sqrt{h\sum_{j=1}^{N}\left|u_j^{\text{exact}} - (u_N)_j\right|^2}, \quad L_\infty = \left\|u^{\text{exact}} - u_N\right\|_\infty \simeq \max_j \left|u_j^{\text{exact}} - (u_N)_j\right|. \tag{31}$$

to check the distinction between the computational and exact solutions for $j = 1, 2, \ldots, N$. Also, we obtained the following two conserved quantities in §4:

$$\begin{aligned} C_1 &= \int_a^b \left(-\frac{1}{1+2p}bu^{1+2p} - \frac{1}{4}au_x^2 + \frac{1}{4}auu_{xx} - \frac{1}{3}uu_{xx}\right)\mathrm{d}x \\ &\simeq h\sum_{j=1}^{N}\left[-\frac{1}{1+2p}b\left(u_j^n\right)^{1+2p} - \frac{1}{4}a\left(u_j^n\right)_x^2 + \frac{1}{4}a\left(u_j^n\right)\left(u_j^n\right)_{xx} - \frac{1}{3}\left(u_j^n\right)\left(u_j^n\right)_{xx}\right], \\ C_2 &= \int_a^b \left(-\frac{1}{1+2p}bu^{a-1}u^{1+2p} - \frac{1}{4}au^{a-1}u_x^2 + \frac{1}{4}auu^{a-1}u_{xx} - \frac{1}{3}u^a u_{xx}\right)\mathrm{d}x \\ &\simeq h\sum_{j=1}^{N}\left[-\frac{1}{1+2p}b\left(u_j^n\right)^{a-1}\left(u_j^n\right)^{1+2p} - \frac{1}{4}a\left(u_j^n\right)^{a-1}\left(u_j^n\right)_x^2 + \frac{1}{4}a\left(u_j^n\right)\left(u_j^n\right)^{a-1}\left(u_j^n\right)_{xx} - \frac{1}{3}\left(u_j^n\right)^a\left(u_j^n\right)_{xx}\right] \end{aligned} \tag{32}$$

to investigate the difference in conserved quantities during the wave motion and validity of the applied method.

5.4.1 *Non-topological solitary wave solution.*

Firstly, propagation of the non-topological solitary wave is investigated by using the generalized Vakhnenko–Parkes (gVP) equation (2). Here, we use the non-topological solitary wave solution [10] of the gVP equation (2) for the comparison of exact and approximate results

$$u(x,t) = A\,\mathrm{sech}^{\frac{2}{2p-1}}\left[B\left(x - x_0 - ct\right)\right], \tag{33}$$

where

$$B = \left[\frac{b\left(2p-1\right)A^{2p-1}}{2\left(2p+1\right)}\right]^{\frac{1}{2}}, \quad a = -1, \quad b > 0. \tag{34}$$

We need boundary and initial conditions as

$$\begin{aligned} &u_N(-300,t) = 0, \qquad u_N(300,t) = 0, \\ &(u_N)_x(-300,t) = 0, \qquad (u_N)_x(300,t) = 0, \quad t > 0 \end{aligned} \tag{35}$$

and

$$u(x,0) = A\,\mathrm{sech}^{\frac{2}{2p-1}}\left[B\left(x - x_0\right)\right] \tag{36}$$

to solve eq. (2).

5.4.2 *Topological solitary wave solution.*

Secondly, dispersion of the topological solitary wave is investigated by utilising the gVP equation (2). Here, we use the topological solitary wave solution [10] of the gVP equation (2) for the comparison of numerical and analytical solutions

$$u(x,t) = A\tanh\left[B\left(x - x_0 - ct\right)\right], \tag{37}$$

where

$$B = \sqrt{-\frac{b}{4}}A, \quad a = -1, \quad b < 0. \tag{38}$$

To figure out eq. (2), the boundary and initial guesses are taken as

$$\begin{aligned} &u_N(-250,t) = 0, \qquad u_N(250,t) = 0, \\ &(u_N)_x(-250,t) = 0, \qquad (u_N)_x(250,t) = 0, \quad t > 0 \end{aligned} \tag{39}$$

and

$$u(x,0) = A\tanh\left[B\left(x - x_0\right)\right], \tag{40}$$

respectively.

5.4.3 *Physical interpretation of the obtained results.*

In this subsection, we interpret the results obtained for the VP equation. We execute the algorithm up to $t = 5$ with the parameters $a = -1$, $b = 0.1$, velocity $c = 0.2$, amplitude $A = 0.5$, $\Delta x = 0.1$, $\Delta t = 0.1$ over the interval $[-300, 300]$ for different values of p, respectively. The percentages of relative variations of the conserved quantities C_1 and C_2 are measured as 3.538×10^{-11} and 6.094×10^{-9} for $p = 1$; 4.330×10^{-10} and 4.590×10^{-8} for $p = 2$; 2.379×10^{-10} and 1.592×10^{-11} for $p = 3$, respectively. The calculated results for the conserved quantities and error norms for the motion of non-topological solitary waves are presented in table 2

Table 2. The conserved quantities and error norms for motion of the non-topological solitary waves.

p	t	C_1	C_2	L_2 Error	L_∞ Error
1	0	−0.0284001189	110.1480596664	0.000000000000	0.000000000000
	1	−0.0284001189	110.1480596765	3.120336×10^{-2}	7.026890×10^{-3}
	2	−0.0284001189	110.1480596389	6.239932×10^{-2}	1.405144×10^{-2}
	3	−0.0284001189	110.1480596114	9.358043×10^{-2}	2.107130×10^{-2}
	4	−0.0284001189	110.1480596409	1.247392×10^{-1}	2.808413×10^{-2}
	5	−0.0284001189	110.1480596597	1.558684×10^{-1}	3.508759×10^{-2}
2	0	−0.0088015010	115.0105765914	0.000000000000	0.000000000000
	1	−0.0088015010	115.0105766018	1.737127×10^{-2}	2.329949×10^{-3}
	2	−0.0088015010	115.0105766071	3.474197×10^{-2}	4.659785×10^{-3}
	3	−0.0088015010	115.0105766054	5.211152×10^{-2}	6.989393×10^{-3}
	4	−0.0088015010	115.0105766142	6.947920×10^{-2}	9.318646×10^{-3}
	5	−0.0088015010	115.0105766441	8.684433×10^{-2}	1.164742×10^{-2}
3	0	0.0133231242	115.0701528551	0.000000000000	0.000000000000
	1	0.0133231242	115.0701528551	1.044878×10^{-2}	8.790785×10^{-4}
	2	0.0133231242	115.0701528551	2.089751×10^{-2}	1.758149×10^{-3}
	3	0.0133231242	115.0701528551	3.134610×10^{-2}	2.637204×10^{-3}
	4	0.0133231242	115.0701528551	4.179450×10^{-2}	3.516236×10^{-3}
	5	0.0133231242	115.0701528551	5.224265×10^{-2}	4.395236×10^{-3}

for $p = 1, 2, 3$. Observations from the initial stage up to time $t = 5$ are detailed in the table. Given that Δt is sufficiently small, the corresponding error norms are quite minimal. The motion of the solitary waves and their contour plots can be observed in figure 4 for $p = 1, 2, 3$. These waves exhibit a bell-shaped profile and maintain their speed. Figure 4 shows the changes in the structure of non-topological solitary waves caused by the nonlinearity effect when the amplitude is kept constant. It is seen that the wave becomes wider as the degree of nonlinearity increases. The nonlinearity effect can spread the energy of the wave to different areas, which leads to the widening of the wave base. Even if the amplitude is kept constant, the distribution of the wave energy over a wider area widens the wave profile. A two-dimensional view of the solution profiles can be seen in figure 5a for $p = 1, 2, 3$. Figure 5a also shows that the wave base widens as the degree of nonlinearity increases. The widening of the wave base means that the wave effect spreads over a wider area, which leads to a more stable and accurate numerical solution. As can be seen from figure 5b, when the wave spreads over a wider area, the absolute error decreases. Considering the contribution of the conserved quantities, the results are depicted in figure 6 for $p = 1, 2, 3$. Upon examining figure 6, we observe that the curves representing conserved quantities for the motion of non-topological solitary waves flatten as the degree of nonlinearity increases.

Another family of solutions in this context is the topological solitary waves. The computation is performed up to time $t = 5$ with the parameters $a = -1$, $b = -0.1$, velocity $c = 0.2$ and amplitude $A = 0.4$ over the interval $[-250, 250]$ for different values of Δx and Δt, respectively. The percentages of relative variations of the conserved quantities C_1 and C_2 are measured as 3.738×10^{-13} and 2.539×10^{-2} for $\Delta x = 0.2$ and $\Delta t = 0.1$; 1.310×10^{-12} and 7.141×10^{-2} for $\Delta x = 0.1$ and $\Delta t = 0.02$, respectively. Table 3 presents the error norms and conserved quantities for the motion of the topological solitary waves. The stability of the calculated conserved quantities is evident when the spatial step size is chosen to be $\Delta x = 0.2$, $\Delta t = 0.1$ by setting the final time $t = 5$. Furthermore, we observe that the error decreases when the mesh is refined with $\Delta x = 0.1$, $\Delta t = 0.02$. Graphical results in this case can be seen in figure 7 by considering different parameter values. Choosing $\Delta x = 0.2$, $\Delta t = 0.1$, the results correspond to figure 7a along with the contour plot in figure 7b. By changing the parameter values to $\Delta x = 0.1$, $\Delta t = 0.02$, the results are shown in figure 7c along with the contour plot in figure 7d. A two-dimensional view of the solution profiles can be seen in figure 8a for different values of Δx and Δt. The corresponding absolute error plot is shown in figure 8b. Keeping into view the contribution of conserved quantities, the results can be seen in figure 9 for different values of Δx and Δt.

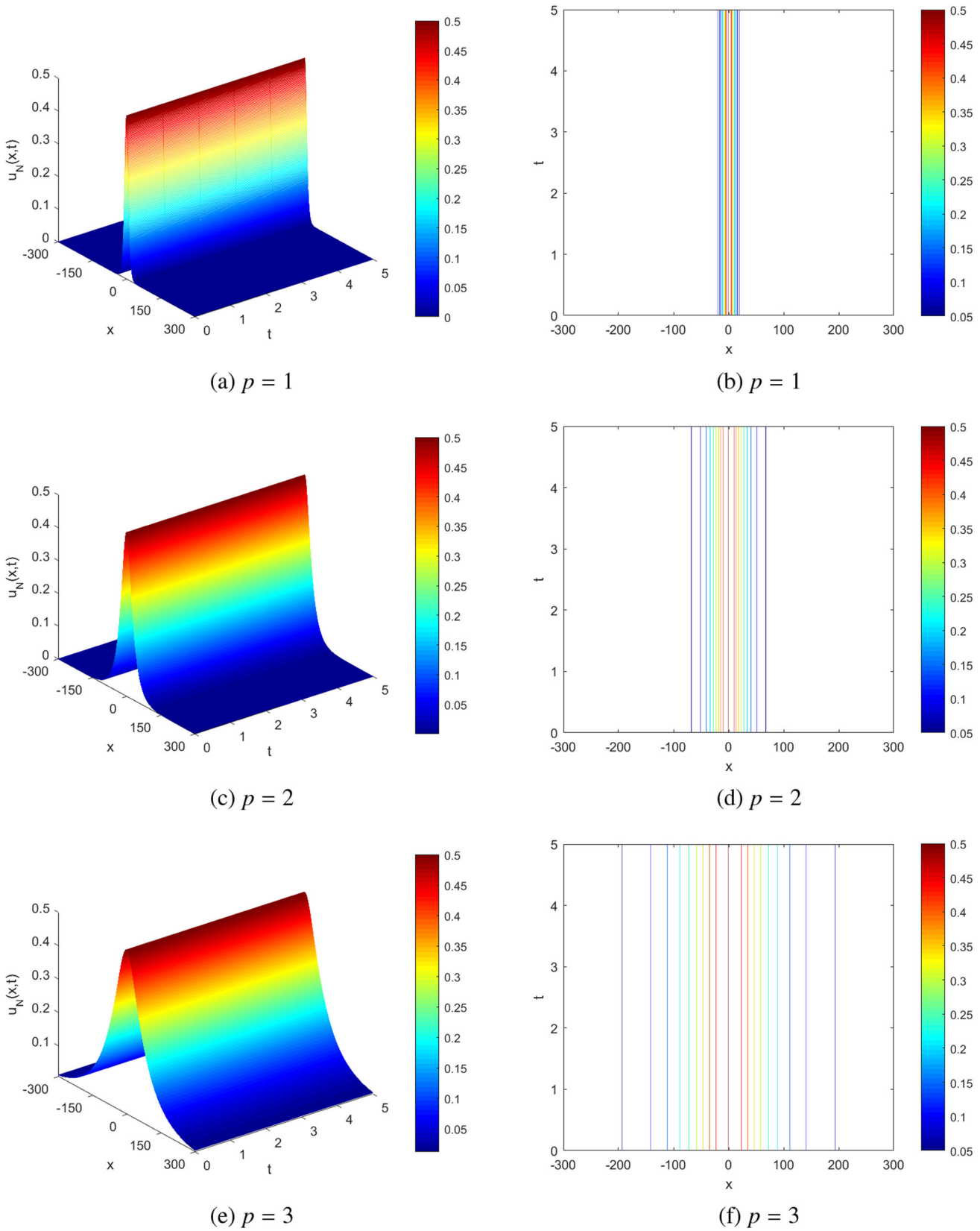

Figure 4. Motion of the non-topological solitary waves and their contours for $p = 1, 2, 3$.

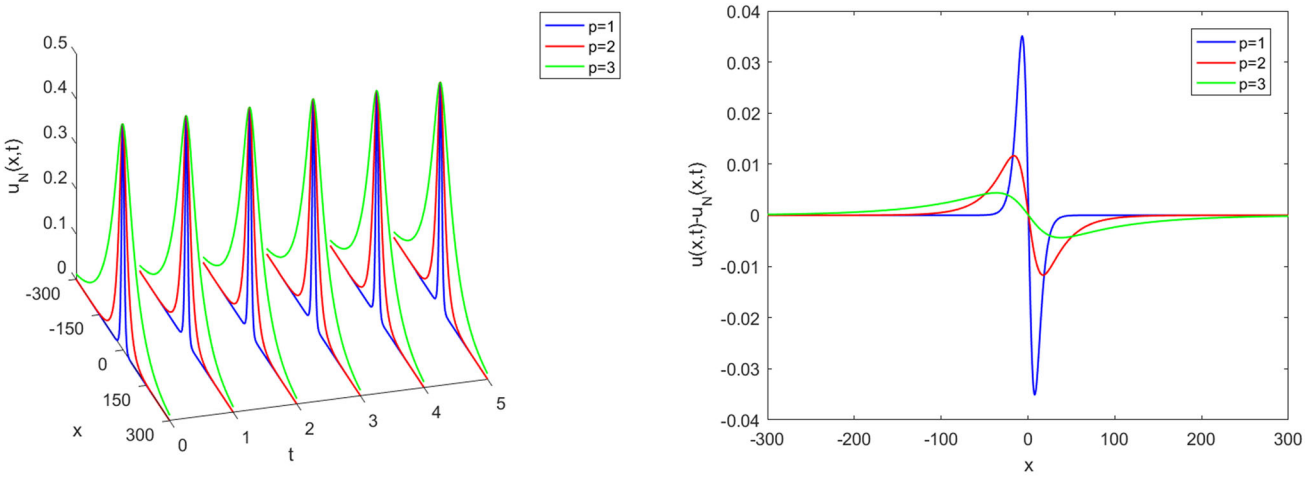

(a) (b)

Figure 5. Motion of the non-topological solitary waves and absolute errors for $p = 1, 2, 3$ at $t = 5$. (**a**) Non-topological solitary waves and (**b**) absolute errors.

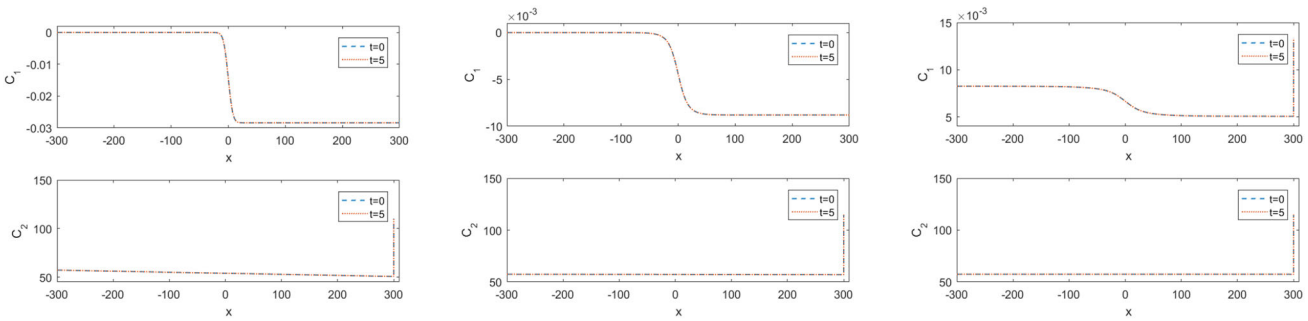

(a) $p = 1$ (b) $p = 2$ (c) $p = 3$

Figure 6. Conserved quantities for the motion of the non-topological solitary waves for $p =$ (**a**) 1, (**b**) 2 and (**c**) 3.

Table 3. The conserved quantities and error norms for the motion of the topological solitary waves.

Δx, Δt	t	C_1	C_2	L_2 Error	L_∞ Error
$\Delta x = 0.2$	0	9.5043870820	7099.7105453125	0.000000000000	0.000000000000
$\Delta t = 0.1$	1	9.5043870820	7099.3023194537	2.323121×10^{-2}	5.059383×10^{-3}
	2	9.5043870820	7100.8062723981	4.646173×10^{-2}	1.011875×10^{-2}
	3	9.5043870820	7101.0449907881	6.969072×10^{-2}	1.517654×10^{-2}
	4	9.5043870820	7100.8813158258	9.291748×10^{-2}	2.023426×10^{-2}
	5	9.5043870820	7101.5130216253	1.161413×10^{-1}	2.528884×10^{-2}
$\Delta x = 0.1$	0	18.7043231377	805.9331096001	0.000000000000	0.000000000000
$\Delta t = 0.02$	1	18.7043231377	806.4467385514	2.323095×10^{-2}	5.059518×10^{-3}
	2	18.7043231377	806.5577519774	4.646135×10^{-2}	1.011868×10^{-2}
	3	18.7043231377	806.8664779090	6.969018×10^{-2}	1.517700×10^{-2}
	4	18.7043231377	806.7723088675	9.291698×10^{-2}	2.023416×10^{-2}
	5	18.7043231377	806.5086132454	1.161409×10^{-1}	2.528972×10^{-2}

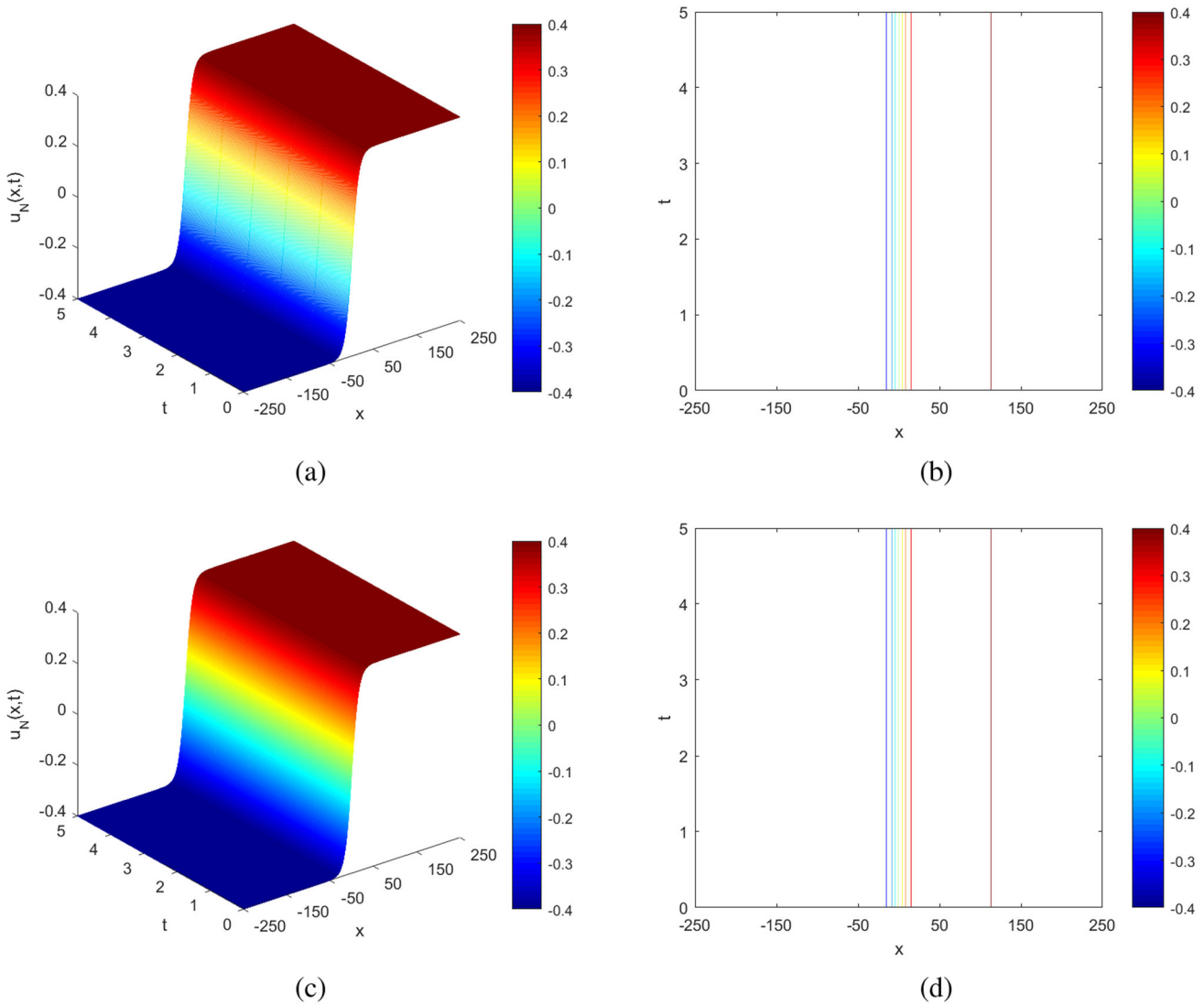

Figure 7. Motion of the topological solitary waves and their contours for different values of Δx and Δt. (**a**) $\Delta x = 0.2$, $\Delta t = 0.1$, (**b**) $\Delta x = 0.2$, $\Delta t = 0.1$, (**c**) $\Delta x = 0.1$, $\Delta t = 0.02$ and (**d**) $\Delta x = 0.1$, $\Delta t = 0.02$.

6. Discussion

Our findings exhibit perfect alignment with those documented in the existing literature [1,2,4,12]. These studies have established benchmarks for the VP equation and our results corroborate with their theoretical and numerical findings.

The results presented in this study hold significant potential for application in various physical systems, particularly in fields, such as fluid dynamics and plasma physics. To validate the proposed solutions, the experimental set-ups include wave tanks for fluid dynamics and plasma chambers for exploring plasma physics. These experimental environments would facilitate the observation of solitary wave propagation and the measurement of wave profiles, enabling direct comparisons with our theoretical and numerical findings. Furthermore, incorporating high-speed cameras and sensitive detectors would be crucial for capturing the dynamic behaviour of solitary waves.

7. Conclusion

The primary objective of this work is to develop a hybrid computational scheme for the numerical solution of the VP equation. To achieve this objective, we employed B-spline functions within a finite-element approach. Conducting stability analysis ensured the unconditional stability of our proposed scheme. To validate its efficacy, various test cases were examined,

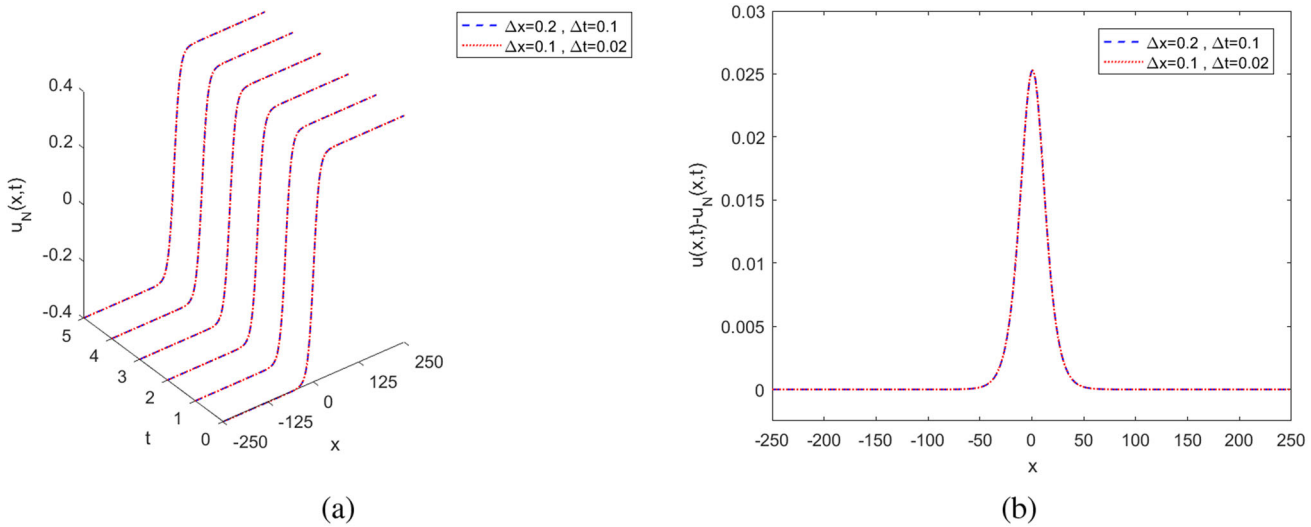

Figure 8. Motion of (**a**) topological solitary waves and (**b**) absolute errors at $t = 5$ for different values of Δx and Δt.

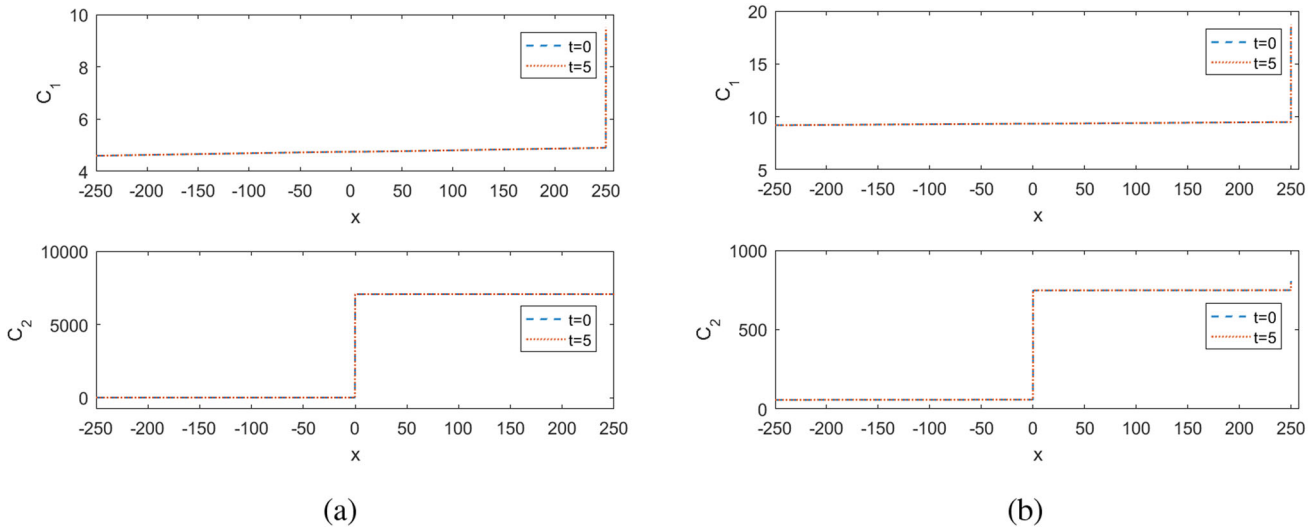

Figure 9. Conserved quantities for the motion of the topological solitary waves for different values of Δx and Δt. (a) $\Delta x = 0.2$, $\Delta t = 0.1$ and (b) $\Delta x = 0.1$, $\Delta t = 0.02$.

encompassing parameter variations and subsequent calculations. Additionally, alongside the numerical results, an analytical solution was derived using the Khater II technique, followed by computations of conservation laws. All findings exhibit perfect alignment with those documented in the existing literature. Currently, we are actively pursuing the extension of our proposed algorithm to address other nonlinear evolution problems within this class.

References

[1] G L Lamb Jr, *J. Math. Phys.* **15**(**12**), 2157 (1974)
[2] V O Vakhnenko and E J Parkes, *Nonlinearity* **11**(**6**), 1457 (1998)
[3] V O Vakhnenko, E J Parkes and A J Morrison, *Chaos Solitons Fractals* **17**(**4**), 683 (2003)
[4] W-X Ma and E Fan, *Comput. Math. Appl.* **61**(**4**), 950 (2011)

[5] V O Vakhnenko and E J Parkes, *Adv. Math. Phys.* **2016**, 2916582 (2016)
[6] A Tripathy and S Sahoo, *Int. J. Mod. Phys. B* **37**(**32**), 2350286 (2023)
[7] X H Liu and C He, (2013) *ISRN Math. Phys.* **2013**, 178648
[8] A J Morrison, E J Parkes and V O Vakhnenko, *Nonlinearity* **12**(**5**), 1427 (1999)
[9] Y Ye, J Song, S Shen and Y Di, *Results Phys.* **2**, 170 (2012)
[10] F Majid, H Triki, T Hayat, OMM Aldossary and A Biswas, *Nonlinear Anal Modelling Control* **17**, 60 (2012)
[11] Y Ma, B Li and C Wang, *Appl. Math. Comput.* **211**(**1**), 102 (2009)
[12] A-M Wazwaz, *Chin. J. Phys.* **57**, 375 (2019)
[13] S C Anco and G Bluman, *Eur. J. Appl. Math.* **13**(**5**), 567 (2002)
[14] D Poole and W Hereman, *Appl. Anal.* **89**(**4**), 433 (2010)
[15] S Dhawan, S Kapoor and S Kumar, *J. Comput. Sci.* **3**(**5**), 429 (2012)
[16] S Dhawan, S Kapoor and S Kumar, *Appl. Math. Comput.* **261**, 128 (2015)
[17] T Ak, S Dhawan, S B G Karakoc, S K Bhowmik and K R Raslan, *Math. Modelling Anal.* **22**(**3**), 373 (2017)
[18] P M Prenter, *Splines and variational methods* (John Wiley, 1975)

Springer Nature or its licensor (e.g. a society or other partner) holds exclusive rights to this article under a publishing agreement with the author(s) or other rightsholder(s); author self-archiving of the accepted manuscript version of this article is solely governed by the terms of such publishing agreement and applicable law.